PHYSICAL REVIEW B **92**, 014425 (2015)

Quantum oscillations and magnetic reconstruction in the delafossite $PdCrO_2$

Clifford W. Hicks,[1,2] Alexandra S. Gibbs,[1,3,4] Lishan Zhao,[1,2] Pallavi Kushwaha,[2] Horst Borrmann,[2] Andrew P. Mackenzie,[1,2,*] Hiroshi Takatsu,[5] Shingo Yonezawa,[6] Yoshiteru Maeno,[6] and Edward A. Yelland[1,7]

[1]*Scottish Universities Physics Alliance (SUPA), School of Physics and Astronomy, University of St Andrews, St Andrews KY16 9SS, United Kingdom*

[2]*Max Planck Institute for Chemical Physics of Solids, Nöthnitzer Str. 40, 01187 Dresden, Germany*

[3]*School of Chemistry and EaStCHEM, University of St Andrews, North Haugh, St Andrews KY16 9ST, United Kingdom*

[4]*Max Planck Institute for Solid State Research, Heisenbergstrasse 1, 70569 Stuttgart, Germany*

[5]*Department of Physics, Tokyo Metropolitan University, Tokyo 192-0397, Japan*

[6]*Department of Physics, Graduate School of Science, Kyoto University, Kyoto 606-8502, Japan*

[7]*SUPA, School of Physics and Astronomy, and Centre for Science at Extreme Conditions, University of Edinburgh, Mayfield Road, Edinburgh EH9 3JZ, United Kingdom*

(Received 16 April 2015; revised manuscript received 28 May 2015; published 29 July 2015)

We report quantum oscillation data on the metallic triangular antiferromagnet $PdCrO_2$. We find that, to very high accuracy, the observed frequencies of $PdCrO_2$ can be reproduced by reconstruction of the (nonmagnetic) $PdCoO_2$ Fermi surface into a reduced zone. The reduced zone corresponds to a magnetic cell containing six chromium sites, giving a $\sqrt{3} \times \sqrt{3}$ in-plane reconstruction, and $\times 2$ interplane reconstruction. The interplane ordering represents a reduction in lattice symmetry, possibly to monoclinic, and an associated lattice distortion is expected. In addition, we report a magnetic transition under an applied in-plane field that is probably equivalent to the spin-flop transition reported for $CuCrO_2$, and present data on its field-angle dependence. We also report measurements of the resistivity of $PdCrO_2$ up to 500 K.

DOI: 10.1103/PhysRevB.92.014425 PACS number(s): 71.18.+y, 75.30.Kz, 75.50.Ee

Magnetic ions coordinated on a triangular lattice often yield interesting magnetic properties. A prominent example is the insulating CrO_2 sheet, stabilized in materials such as $LiCrO_2$ and $PdCrO_2$. In these compounds, the Cr formal charge is +3, and its configuration is $3d^3$. The crystal field at the Cr sites is nearly octahedral, inducing a gap between the quasi-t_{2g} (d_{xy}, d_{xz}, and d_{yz}) and quasi-e_g ($d_{3z^2-r^2}$ and $d_{x^2-y^2}$) bands. The e_g bands lie above the Fermi level, and the t_{2g} bands are half-filled. The CrO_2 sheet is a Mott insulator: strong Hund's rule coupling aligns the spins on each Cr site, giving a total spin on each Cr site of nearly $\frac{3}{2}$. The CrO_2 sheet is a Heisenberg system, that orders at low temperatures into the 120° triangular Néel phase.

Of materials containing such a CrO_2 sheet, $AgCrO_2$, $CuCrO_2$, and $PdCrO_2$ have the delafossite crystal structure, while $LiCrO_2$, $NaCrO_2$, and $KCrO_2$ have the closely related ordered rock salt structure. All of these systems show 120° order, with the Néel temperature depending strongly on the Cr-Cr spacing. The ordered rock-salt structure gives substantially smaller interplane spacings than the delafossite structure, and somewhat higher Néel temperatures [1].

The interlayer order is a more subtle problem than the intralayer order: in all of these systems the Cr sheets are stacked rhombohedrally, so the molecular fields from first- and second-neighboring layers cancel, and the ordering is determined by more subtle interactions susceptible to perturbation. The interlayer order has observable consequences: $AgCrO_2$ and $CuCrO_2$ show spin-driven ferroelectricity, while $NaCrO_2$ and $LiCrO_2$ do not [2]. $AgCrO_2$ and $CuCrO_2$ have the delafossite structure and $NaCrO_2$ and $LiCrO_2$ the ordered rock-salt structure, but the more essential difference appears to be the interlayer order: in $AgCrO_2$ [3] and $CuCrO_2$ [4,5], the interlayer ordering is ferroic, in that the vector chirality, the rotational sense of the spin helices that comprise the 120° phase, is the same in all layers. In $LiCrO_2$, in contrast, neutron scattering data suggest that the vector chirality alternates from layer to layer [6], while the interplane order of $NaCrO_2$ is not clear [7].

This paper focuses on $PdCrO_2$. The Néel temperature of $PdCrO_2$ is $T_N = 37.5$ K, and, like $LiCrO_2$, the vector chirality probably alternates from layer to layer [1,8], so this feature is not restricted to the ordered rock-salt structure.

Whereas the other compounds discussed above are insulators, $PdCrO_2$ is a metal [9], due to Pd $4d/5s$ conduction. The isostructural, nonmagnetic compound $PdCoO_2$ also has the Pd sheets, and its carrier mobility was found to exceed that of copper [10]. In $PdCoO_2$, the strongest d contribution appears to be from the $4d_{z^2}$, however, the relative weight of this and Pd $5s$ at the Fermi level is not clear [11,12]. $PdCrO_2$, therefore, is an interesting system, comprised of highly conducting sheets interleaved with Mott insulating spacer layers. The resistivity anisotropy (ρ_c/ρ_{ab}) is about 180 at 295 K, and about 290 at 50 K [13]. It would be interesting to determine whether the metallic Pd conduction has any effect on the magnetic order.

What is certainly true is that the Pd conduction can be used as a probe of the magnetic order. Quantum oscillation [14] and angle-resolved photoemission spectroscopy (ARPES) [15,16] studies have shown that the $PdCrO_2$ Fermi surfaces result from reconstruction of the $PdCoO_2$ Fermi surface into the magnetic zone. Observation of an unconventional anomalous Hall effect

*apm9@st-andrews.ac.uk

in $PdCrO_2$ indicates further that the Cr spins are not coplanar [17].

In this paper, we present measurements of quantum oscillations in $PdCrO_2$, and confirm the overall frequencies reported in Ref. [14]. We add greater resolution and a careful comparison with the nonmagnetic $PdCoO_2$ Fermi surface: we show that reconstruction of the $PdCoO_2$ Fermi surface reproduces most of the observed oscillation frequencies to very high accuracy: the $PdCrO_2$ frequencies can be analyzed in detail without recourse to density functional theory calculations. We show that the magnetic coupling is k_z dependent: it is much weaker at $k_z = \pm\pi$ than at $k_z = 0$. Also, the dominant magnetic scattering vectors are those corresponding to a 6-Cr magnetic unit cell giving a $\times 2$ interplane reconstruction in addition to the $\sqrt{3} \times \sqrt{3}$ in-plane reconstruction. The interplane order represents a reduction in lattice symmetry, from $R\bar{3}m$ (rhombohedral) to, for the highest-symmetry possibility, $C2/c$ (monoclinic).

We also report a magnetic transition under applied field, at a similar field to a spin-flop transition reported in $CuCrO_2$, that was observed in the course of measurement of the oscillations. Finally, we present measurements of the resistivity of $PdCrO_2$ to high temperatures.

I. METHODS

Single crystals of $PdCrO_2$ were grown by a NaCl flux method, using $PdCrO_2$ powder synthesized via a solid-state reaction [18]. We measured magnetic oscillations in two samples of $PdCrO_2$, by torque magnetometry, using the same piezoresistive AFM cantilevers as in our previous study on $PdCoO_2$ [10,19]. The cantilevers were mounted on rotatable platforms with integrated field angle sensors. Some raw data for sample #1 are shown in Fig. 1.

Sample #1 was roughly $230 \times 300 \times 11$ μm, and sample #2 $160 \times 100 \times 15$ μm. For sample #1, the field was rotated about a $\langle 1000 \rangle$ axis (using hexagonal indexing), and for sample #2 a $\langle 1\bar{1}00 \rangle$ axis; these axes are illustrated at the bottom right of Fig. 2. Both samples showed strong low-frequency oscillations ($\sim$800 T for field angle $\theta \to 0$) that dominate the data. In sample #1, at 0.7 K these oscillations were discernible at fields as low as 2 T. At high fields (above $\sim$10 T), the oscillation amplitude was very large, leading to strong torque interaction: the oscillations had a triangular form, and strong sum and difference frequencies appeared in the Fourier transforms. While torque interaction complicates the analysis somewhat, it may be difficult to avoid if the samples are to be large enough for higher-frequency oscillations to be resolved.

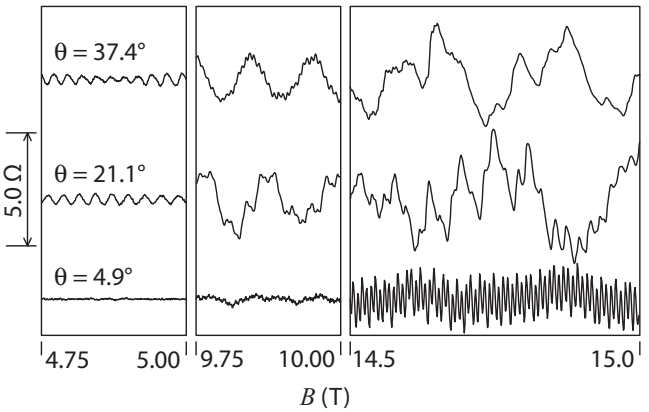

FIG. 1. Magnetic oscillations in sample #1 at three field angles. The y scale is the resistance of the piezoresistive sense element on the cantilever.

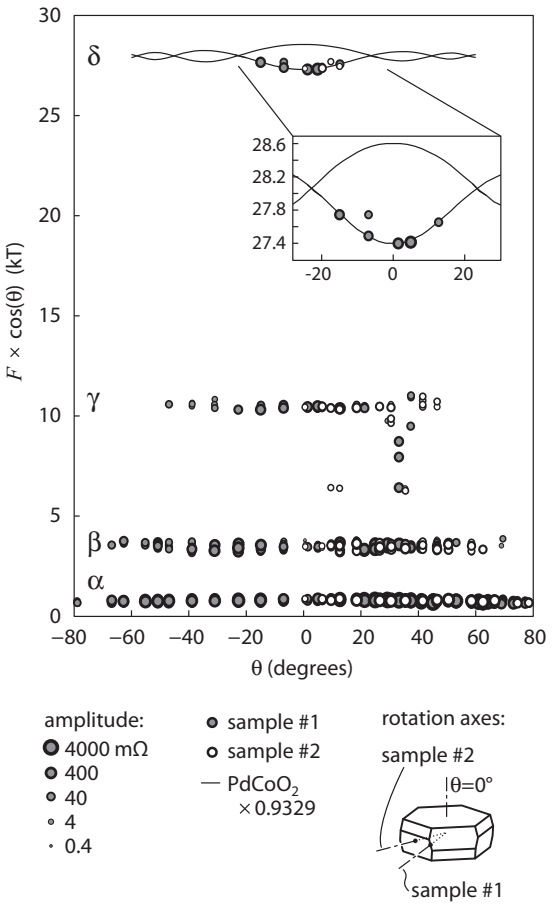

FIG. 2. The observed oscillation frequencies of $PdCrO_2$, multiplied by $\cos(\theta)$, against field angle θ. The field rotation axes are shown at bottom right, referenced to the nonmagnetic zone. The frequencies are from Fourier transformation of the data over the range 4.2 to 15 T. Frequencies that are clearly sum or difference frequencies are not shown. The indicated amplitudes of the oscillations are peak-to-peak amplitudes of the resistance of the sense element on the cantilever. The $PdCoO_2$ frequencies are taken from the model in Ref. [10], and have been scaled by 93.3%.

The oscillation amplitudes were history dependent. Cooling the sample through T_N in a 15-T field resulted in oscillation amplitudes for the α, β, and γ orbits (illustrated in Fig. 3) roughly four times as large as with zero-field cooling. These large amplitudes persisted as long as the field was maintained. Releasing the field and heating the sample to $\sim$1 K caused the amplitudes to decrease, and reapplying fields up to 15 T did not recover the large amplitudes. The system therefore appears to be nonergodic. A possible origin of glassy behavior is domain-boundary Cr spins: the relatively large magnetic unit cell of $PdCrO_2$ means that in the absence of training a complex domain structure is likely.

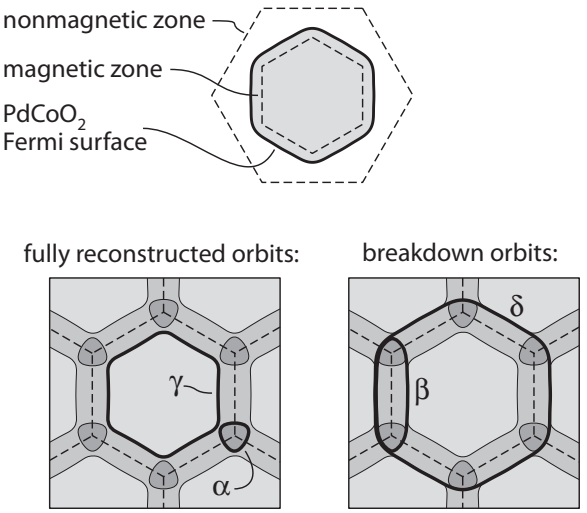

FIG. 3. A two-dimensional (2D) model of the reconstruction. Top: the $PdCoO_2$ Fermi surface in the 2D nonmagnetic zone, and magnetic zone arising from a $\sqrt{3} \times \sqrt{3}$ reconstruction. Bottom: reconstruction into the magnetic zone. The fully reconstructed orbits α and γ are illustrated in the left-hand panel, and the breakdown orbits β and δ in the right-hand panel.

For measurement of the temperature dependence of the oscillation amplitudes, we cooled the sample in a field and kept the field above 8 T at all times, to maintain large oscillation amplitudes. For measurement of the angle dependence of the frequencies, torque interaction was a greater concern, and the sample was cooled through T_N in zero field.[1]

II. RESULTS: THE OSCILLATIONS

The oscillation frequencies as a function of field angle are shown in Fig. 2. Four sets of intrinsic peaks can be identified, located, at $\theta = 0$, at around 0.8, 3.5, 10.5, and 27.4 kT. Following Ref. [14], we label these α, β, γ, and δ. All the frequencies scale broadly as $1/\cos(\theta)$, indicating that the Fermi surfaces are highly two dimensional.[2]

It has been established that the $PdCrO_2$ orbits result from a $\sqrt{3} \times \sqrt{3}$ reconstruction of the $PdCoO_2$ Fermi surface, due to the 120° Néel order [14,16]. This reconstruction is illustrated in Fig. 3. The α and γ orbits are fully reconstructed orbits, while β and δ result from magnetic breakdown, i.e., the orbits cross gaps in k space.

The cyclotron masses were determined for sample #1 by Lifshitz-Kosevich fits to the temperature dependence of the amplitudes. We analyzed the data between 7.5 and 11.5 T, avoiding higher fields where torque interaction was very strong, and verified that within this range there was no systematic variation of the masses with field.

TABLE I. Observed frequencies at $\theta = 0$, and expected frequencies from two-dimensional $\sqrt{3} \times \sqrt{3}$ reconstruction of the $PdCoO_2$ $k_z = 0$ and $k_z = \pm\pi$ orbits. Boldface indicates a better match to observations. In the calculations, the $PdCoO_2$ frequencies are scaled by 93.3%, and avoided crossings at band crossings are neglected (apart from their effect on Fermi surface topology).

	α_3	β	γ	δ
Observed frequencies (kT)	0.87	3.45	10.52	27.40
Calc'd $k_z = 0$ freq's (kT)	**0.91**	3.92	**10.50**	28.60
Calc'd $k_z = \pi$ freq's (kT)	0.69	**3.36**	11.27	**27.40**

The masses obtained for the α, β, γ, and δ orbits are (0.33 ± 0.01), (0.84 ± 0.01), (1.37 ± 0.02), and $(1.55 \pm 0.04)m_e$, respectively; the fits are shown in the Appendix. These are in good overall agreement with ARPES measurements. A Fermi velocity of 4.2 eV Å was measured, by ARPES, at the corners of the nonmagnetic Fermi surface, and 4.9 eV Å at the faces [16]. If an isotropic Fermi velocity of 4.6 eV Å is taken along the perimeters of the α, β, γ, and δ orbits, masses of 0.34, 0.63, 1.00, and $1.53m_e$ are obtained, respectively: the cyclotron masses from the Lifshitz-Kosevich fits are in very close agreement with the ARPES estimates for α and δ, and ~35% heavier for β and γ.[3]

Also shown in Fig. 2 are the $PdCoO_2$ frequencies from the parametrized model in Ref. [10], for comparison with $PdCrO_2$. To make the comparison, the $PdCoO_2$ frequencies need to be scaled by the square of the ratio of in-plane lattice constants. We found that the best match is obtained with a scaling of 93.3%, which is very close to the expected scaling $(2.830\ \text{Å}/2.923\ \text{Å})^2 = 93.7\%$ [1,20,24].

From the comparison it is apparent that the lower branch of the $PdCoO_2$ frequencies, arising from the neck orbit (i.e., the $k_z = \pm\pi$ orbit), is visible in the $PdCrO_2$ data, while the upper branch, from the belly orbit ($k_z = 0$), is not. This feature is part of a pattern that extends to the other frequencies: the observed breakdown frequencies derive from reconstruction of the nonmagnetic neck orbit, while the observed fully reconstructed frequencies derive mainly from the belly orbit. The pattern is illustrated in Table I, which shows the observed $PdCrO_2$ frequencies (for $\theta \to 0$) and the expected frequencies based on reconstruction of the $PdCoO_2$ neck and belly orbits: the neck reconstruction yields the observed β and δ frequencies, and the belly reconstruction α_3 and γ. (The α frequencies comprise three subbands α_1, α_2, and α_3; we will discuss this in more detail in the following.)

What this pattern means is that the belly orbit sees the magnetic order more strongly than the neck orbit. This is not surprising: the Cr sites are midway between the Pd sheets

[1]While measuring the angle dependence of the oscillations in sample #1, we performed a "de-Gauss" routine at the start of each run, in which the field was ramped to −2 T, then +1 T, then −0.5 T, and so on. The aim was to reduce the probability of the system evolving gradually into a more ordered state, with larger oscillation amplitudes, though it is not clear whether the procedure had much effect.

[2]Some additional peaks appear in the data, between the β and γ frequencies, and are plotted in the figure. It was not obvious in the raw data whether they were real peaks, interaction peaks, or spurious; they are probably spurious.

[3]For calculation of the α and γ expected masses, we use the α_3 and γ_1 orbits.

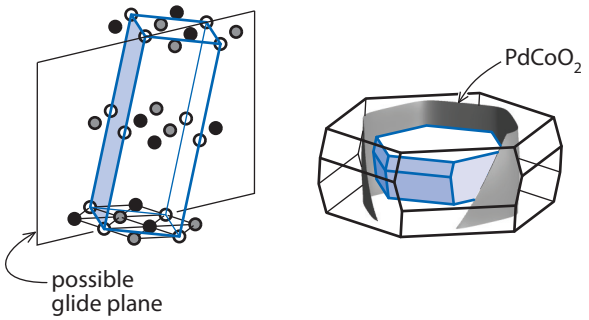

FIG. 4. (Color online) Left: a possible magnetic cell for $PdCrO_2$, that contains 6 Cr sites. The Cr sites are colored black, gray, and white to indicate the three spin directions of each layer. Right: the nonmagnetic first Brillouin zone (black), together with the $PdCoO_2$ Fermi surface and the six-site zone, into which the nonmagnetic Fermi surface is reconstructed.

(which dominate conduction), and the $k_z = \pm\pi$ Bloch states have zero weight at the planes of the Cr nuclei.

It would be interesting to determine whether coupling to the Cr spins affects the quasiparticle masses. The observed δ orbit, located at $k_z = \pm\pi$ and with mass $(1.55 \pm 0.04)m_e$, has a very similar mass to the equivalent orbit in $PdCoO_2$, $(1.45 \pm 0.05)m_e$ [10]. So, apparently, at $k_z = \pm\pi$ the cyclotron mass is not strongly affected by the Cr magnetism. The situation at $k_z = 0$, where the coupling to the Cr spins is stronger, is not clear. The observed γ orbit, which is at $k_z = 0$, has the ~35% mass enhancement noted earlier; but so does the observed β orbit, which is located at $k_z = \pm\pi$.

Overall, then, a two-dimensional $\sqrt{3} \times \sqrt{3}$ reconstruction of the $PdCoO_2$ frequencies, where the reconstruction is weak at $k_z = \pm\pi$, gives a good description of the $PdCrO_2$ frequencies at $\theta = 0$. We now test the reconstruction at other field angles by performing a three-dimensional reconstruction.

We first need a three-dimensional magnetic cell. It must contain at least six Cr sites: three per layer to capture the 120° Néel order, and two layers to capture the alternating vector chirality. The cell we test is shown in Fig. 4.[4] The Cr sites are stacked rhombohedrally, so at T_N there are three equivalent choices for the interplane ordering vector. In choosing one of them, the lattice symmetry is reduced. The space group of the nonmagnetic lattice is $R\bar{3}m$. The highest-symmetry possible magnetic lattice has space group $C2/c$ (base-centered monoclinic): reflection about the glide plane indicated in Fig. 4 reverses the vector chirality within each layer, and translation along the interplane ordering vector restores the

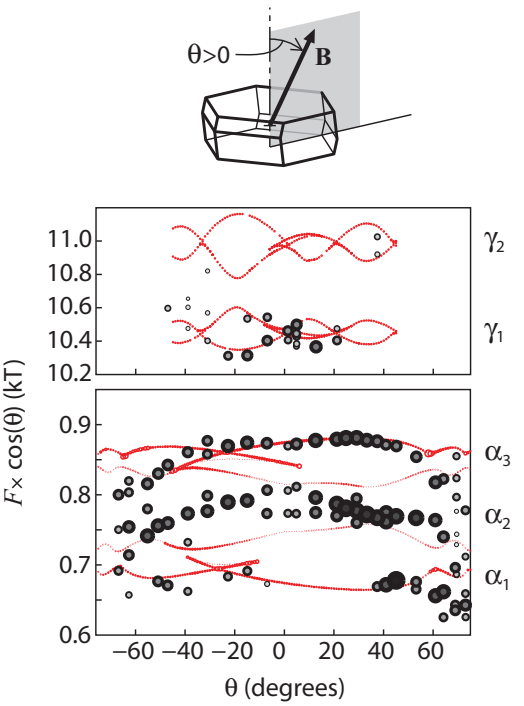

FIG. 5. (Color online) Red circles: calculated frequencies based on reconstruction of the $PdCoO_2$ Fermi surface into the magnetic zone shown in Fig. 4. The upper and lower panels show the γ and α frequencies, respectively. In the lower panel, the diameter of the symbols is proportional to the logarithm of the expected oscillation amplitude, based solely on the curvature of the Fermi surfaces. Black circles: the frequencies observed in sample #1, with the diameter of the symbols proportional to the logarithm of the amplitude.

original lattice.[5] Magnetostructural coupling should lead to a lattice distortion associated with the reduction in symmetry, and it is possible that more subtle features in the magnetic order reduce the symmetry further.

The reconstruction is performed as described in textbooks: sections of the nonmagnetic Fermi surface are translated by combinations of reciprocal lattice vectors of the reduced zone until all portions of the original surface are represented within the reduced zone. For our nonmagnetic surface, we take the parametrized model for the $PdCoO_2$ Fermi surface that was determined in Ref. [10]. The topology of the reconstructed Fermi surfaces is determined by the orientations of the avoided crossings that would occur in the real system, but the calculation does not include finite avoided crossings. Further details of the calculation are given in the Appendix. Our results are shown in Fig. 5, together with the observed frequencies.

There are two γ bands. The lower band γ_1 derives from reconstruction of the belly orbit, and γ_2 the neck orbit. γ_2 is not observed in the data because the magnetic coupling is weak for the neck orbit.

[4]In Refs. [6] ($LiCrO_2$) and [1] ($PdCrO_2$), single-crystal neutron scattering data are analyzed using an 18-site magnetic cell. This is the smallest that can preserve $R\bar{3}m$ symmetry: to preserve $R\bar{3}m$ symmetry the interplane ordering vector must take on all three possibilities in an ABCABC order, so six layers are required to capture both this and the alternating vector chirality. The most-likely magnetic structure that is obtained in Ref. [1] can be reduced to a six-site magnetic cell.

[5]The unit cell shown in Fig. 4 is metrically triclinic (none of the angles are 90°) but if the glide symmetry is preserved, then a 12-site monoclinic supercell can be constructed.

Three α bands appear in the data.[6] The lower and upper bands α_1 and α_3 are reproduced well by the calculation. α_3 is from the nonmagnetic belly orbit and α_1 the neck orbit, so α_1 has a much lower amplitude in the data. The middle band α_2 is not reproduced in the calculations. It could be a breakdown orbit. There are prominent breakdown orbits in the data (β and δ), and the $\times 2$ interplane reconstruction could lead to breakdown orbits that mix segments from the original neck and belly orbits.

For this calculation, we supposed that the system chose the interplane ordering vector that aligned the plane of (possible) glide symmetry with the field rotation plane. The other two possibilities would lead to the glide and rotation planes being separated by 120°. We also calculated this possibility, with the result shown in the Appendix. The match to the data is reasonable but not as good, so it appears that either the glide and rotation planes were aligned by chance, or the fields applied during the measurement reoriented the magnetic reconstruction.

We also show in the Appendix results for a strictly two-dimensional reconstruction, that would preserve the $R\bar{3}m$ symmetry of the nonmagnetic lattice. The results do not match the data well, and we conclude that the dominant magnetic scattering vectors are those of the magnetic cell shown in Fig. 4.

III. SPIN-FLOP TRANSITION

In addition to quantum oscillations, a large-scale feature appeared during the torque magnetometry measurements on sample #1: a first-order magnetic transition. It occurs at a field of around 6.5 T for $\theta = 90°$ (i.e., the field applied in the plane). On the high-field side of the transition, the sample has a much larger c-axis magnetic moment than on the low-field side. Figure 6 shows the set of torque curves obtained in this study, divided by the applied field to yield $M_\perp$, the magnetization perpendicular to the applied field, and smoothed so as to exclude the oscillations and show broad-scale features. The transition and its hysteresis are readily apparent, at $\theta \sim 90°$. It appeared for sample #1 but not #2, so it is sensitive to the direction of the applied field.

Over a small angle range, quantum oscillations were visible both below and above the transition; the Fourier transforms are shown in the Appendix. At each angle within this range, the oscillations have a lower amplitude on the high-field side of the transition than on the low-field side, and the dominant peak shifts to a slightly higher frequency. That the transition affects the oscillations in a consistent manner shows that it is a bulk property.

This transition is at a similar field to a spin-flop transition reported for $CuCrO_2$ [21], 5.3 T for temperatures well below T_N, and probably has the same origin. In $CuCrO_2$, it has been found by single-crystal neutron diffraction that the spins lie in $\langle 0001\rangle$-$\langle 1\bar{1}00\rangle$ planes [5,22,23]. The transition occurs when the field is applied in a $\langle 1\bar{1}00\rangle$ direction, but there is no transition for fields applied in a $\langle 1000\rangle$ direction. It has been shown by symmetry arguments [21] and by direct observation [22] that the transition is a spin flop, where the spin plane rotates by 90°. The spin flop is illustrated in Fig. 7, and discussed in greater detail in Ref. [21].

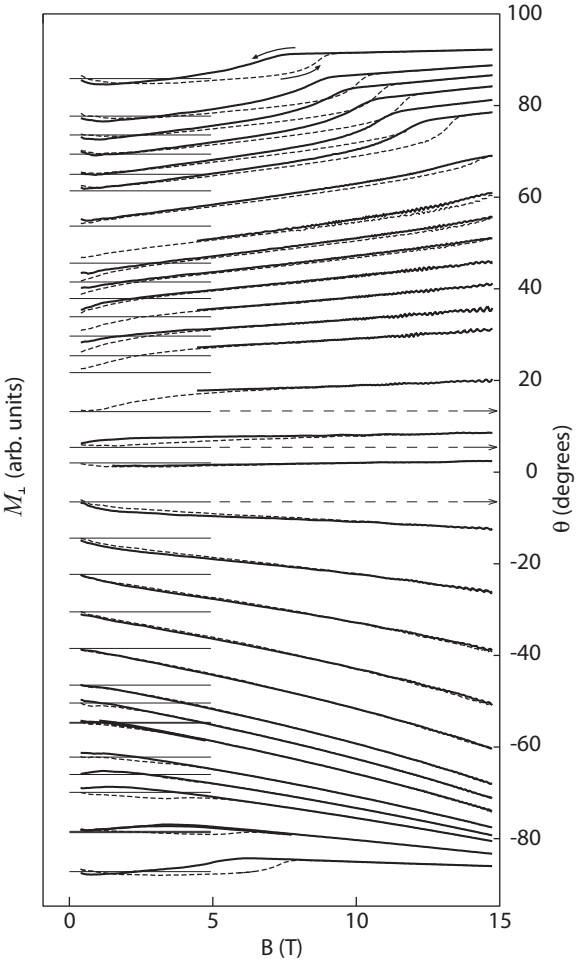

FIG. 6. Perpendicular magnetization against applied field at 0.7 K, for sample #1, where the field was rotated in a $\langle 0001\rangle$-$\langle 1\bar{1}00\rangle$ plane. Each curve is offset by the field angle θ; the offsets are indicated by the thin horizontal lines at the left and the angle scale is on the right. The solid lines show downward field sweeps, the dashed lines upward. The curves are smoothed, to exclude quantum oscillations.

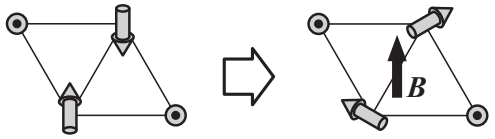

FIG. 7. An illustration of the spin flop. In zero field, the spins lie in $\langle 0001\rangle$-$\langle 1\bar{1}00\rangle$ planes (left panel). When a field is applied in a $\langle 1\bar{1}00\rangle$ direction, the spin plane rotates by 90° (right panel). Note that in $PdCrO_2$ the spins are not perfectly coplanar; see Ref. [1] for details. Also, there may be domains of different $\langle 0001\rangle$-$\langle 1\bar{1}00\rangle$ spin planes; the evolution of each possible domain with applied in-plane field is discussed in Ref. [21].

[6]Ok *et al.* also identify three α bands [14]. However, the frequencies they label α_1 and α_2 are both part of α_2 in our labeling scheme, and Ok *et al.* do not resolve the frequency we label α_1.

For $PdCrO_2$, although observation of an unconventional anomalous Hall effect shows that the spins are not coplanar, neutron scattering data show that the spins lie approximately in a $\langle 0001\rangle$-$\langle 1\bar{1}00\rangle$ plane, similar to $CuCrO_2$. Furthermore, and also as in $CuCrO_2$, the transition occurs when the field is applied in a $\langle 1\bar{1}00\rangle$ direction (sample #1), but not in a $\langle 1000\rangle$ direction (#2). Therefore, the transition is probably the same spin flop.

IV. RESISTIVITY

$PdCoO_2$ has been used as a nonmagnetic analog of $PdCrO_2$ in order to extract the magnetic contribution to the specific heat and electrical resistivity [8,13]. We have shown here that it is a very good comparison: the $PdCrO_2$ Fermi surfaces are, to high precision, a reconstruction of the $PdCoO_2$ Fermi surface, and the cyclotron masses match closely.

The in-plane resistivity of $PdCoO_2$ is substantially nonlinear between ∼100 and 500 K, a feature attributed to prominent optical phonons [24]. The resistivity of $PtCoO_2$ also shows this feature [25]. We include in this paper data on the resistivity of $PdCrO_2$ up to 500 K, in order to extend the comparison reported in Ref. [13] to higher temperatures and to see whether the same feature appears in $PdCrO_2$.

All samples for resistivity measurement were cut with a wire saw into bars of nearly constant width and thickness, and with length-to-width ratios of ∼10, to reduce geometrical uncertainties in conversion of resistance to resistivity. Our data are plotted in Fig. 8. We measured one $PdCoO_2$ and two $PdCrO_2$ samples, labeled A and B; sample A had two pairs of voltage contacts, so in total three $PdCrO_2$ curves were recorded. Averaging the three measurements, the room-temperature (295 K) resistivity of $PdCrO_2$ was found to be $8.2 \pm 1.0\ \mu\Omega\,$cm, where the uncertainty is from uncertainty in the sample dimensions. This is in good agreement with that reported in Ref. [13], 9.4 $\mu\Omega\,$cm.

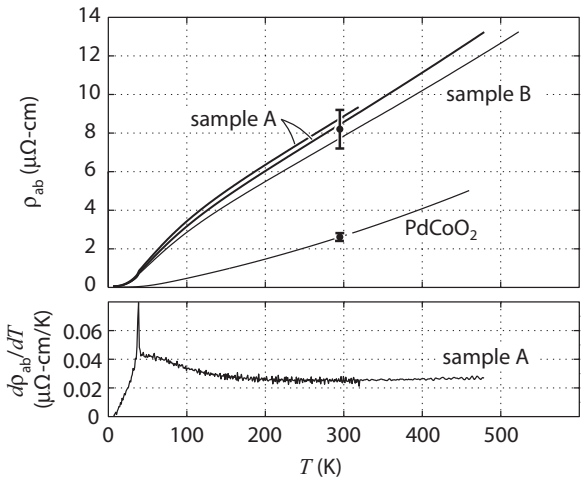

FIG. 8. The resistivity of $PdCrO_2$ against temperature, for two samples. Sample A had two pairs of voltage contacts. The point at 295 K, with error bars, indicates the room-temperature resistivity: $8.2 \pm 1.0\ \mu\Omega\,$cm. Data on a $PdCoO_2$ sample are also shown, scaled to the room-temperature resistivity determined in Ref. [10]: $2.6 \pm 0.2\ \mu\Omega\,$cm. Bottom panel: $d\rho/dT$ for sample A.

The form of the resistivity of $PdCrO_2$ is well established. There is a sharp cusp at T_N, and above T_N the magnetic component of the resistivity ρ_m remains well below its saturation value due to short-range correlation. The increase and eventual saturation of ρ_m as the temperature increases leads to a convex temperature dependence of the resistivity.

The in-plane resistivity of $PdCrO_2$, in contrast to $PdCoO_2$ and $PtCoO_2$, is essentially linear from ∼200 to at least 500 K. It may be that the temperature dependence of ρ_m obscures an optical phonon contribution. ρ_m is expected to saturate when the Cr spins become completely uncorrelated. If ρ_m is estimated by subtracting the resistivity of $PdCoO_2$ from that of $PdCrO_2$, then our data indicate that ρ_m continues to increase at temperatures well above room temperature, i.e., ρ_m continues to evolve to temperatures an order of magnitude greater than T_N. The Weiss temperature of $PdCrO_2$ is ∼−500 K [8], so correlations between the Cr spins are expected to persist to temperatures up to ∼500 K, and a high saturation temperature of ρ_m may be expected.

V. DISCUSSION AND CONCLUSION

The quantum oscillation frequencies indicate that the dominant magnetic scattering vectors are those of a six-site magnetic cell with lower symmetry than the nonmagnetic lattice. An associated lattice distortion is expected to onset at T_N. It has been looked for by both neutron and x-ray diffraction, and not found [1], so any distortion must be small.

The distortion, if it occurs, should resemble that observed in $CuCrO_2$ [26]; there is also evidence for a lattice distortion in $AgCrO_2$ [27]. In $CuCrO_2$, the vector chirality is the same in each layer and the magnetic cell contains three sites [2,4,5]. The magnetic transition is split into two [28], which is expected for easy-axis-type 120° antiferromagnetism: spins first order along the easy axis, then, at a lower temperature, along an in-plane axis. Ultrasound velocity measurements show that the lattice distortion starts at the upper transition, with no apparent anomaly at the lower transition [28].

The transition of $PdCrO_2$ may also be split, although if so the splitting is small and not generally observed in experiment [1]. Either way, the magnetic order implies two separate reductions in symmetry from $R\bar{3}m$: the choice of interplane ordering vector at the (possible) upper transition, and the choice of spin plane at the lower transition (where, again, in $PdCrO_2$ the spins are only approximately coplanar). The two symmetry reductions are likely to couple. The ultrasound data on $CuCrO_2$ suggest that in that system it is the interplane ordering vector that more strongly drives the distortion.

The angle dependence of the spin-flop transition in $PdCrO_2$ is interesting: the transition field appears to vary smoothly from ∼15 T on one side of the plane (at $\theta \sim +55°$) to nearly zero on the other (at $\theta \sim -55°$). At $B = 0$, however, the field angle is a meaningless parameter, so if there is in fact an end point near $B = 0$, then the high- and low-field states are adiabatically connected to each other. Whether this is true and how it might occur for a 90° spin flop requires further investigation.

In summary, $PdCrO_2$ is an interesting system comprised of alternating highly conductive sheets and Mott-insulating spacer layers. It provides a good model for study of the interaction between metallic conduction and antiferromagnetic

order: the conduction is well characterized, arising from a single, open Fermi surface, and much is known about the magnetic order. Also, there are related compounds that permit precise comparisons, such as the nonmagnetic $PdCoO_2$, and other CrO_2-based delafossite and ordered rock-salt materials. Several avenues of inquiry remain open.

ACKNOWLEDGMENTS

We acknowledge useful discussions with J. W. Allen, C. A. Hooley, P. Thalmeier, and B. Schmidt, and practical assistance from N. Nandi. We acknowledge funding from the UK EPSRC, the MEXT KAKENHI (Grant No. 21340100), the Royal Society, the Wolfson Foundation, and the Max Planck Society.

APPENDIX

In this Appendix we first present some supplementary data, and then give further details on the calculation of the three-dimensional reconstruction.

Figure 9 shows the Lifshitz-Kosevich fits to the oscillation amplitudes determined over the field range 8.5–9.5 T. Four such fits were done, over 1-T field ranges starting at 7.5, 8.5, 9.5, and 10.5 T. The masses reported in the main text are the averages of the masses obtained from these fits.

Figure 10 shows the Fourier transforms of the oscillations above and below the putative spin-flop transition, for the narrow angle range over which oscillations were observed on both sides of the transition. On the high-field side of the transition, the oscillations have lower amplitudes and the main peak a higher frequency. (The reduction in amplitude may not be immediately apparent in the figure, but normally quantum oscillation amplitudes grow rapidly as the field is increased, and the reduction in amplitude is very clear in the raw data.)

We now give further details on the reconstruction. The first step is to determine the misalignment, if any, between the sample and the field angle sensor mounted on the rotator platform. This misalignment is determined, for sample #1, by comparison of the observed δ frequencies and the scaled $PdCoO_2$ frequencies, shown in Fig. 2. The best match is obtained when a $0.3 \pm 0.2^\circ$ offset is added to the measured field angle. This is our misalignment, and correction for it is

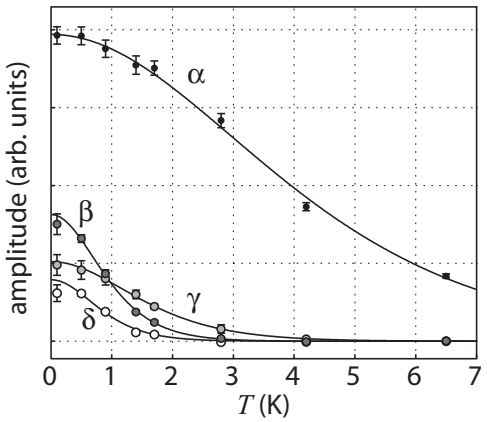

FIG. 9. Lifshitz-Kosevich fits to the amplitudes determined over the field range 8.5–9.5 T.

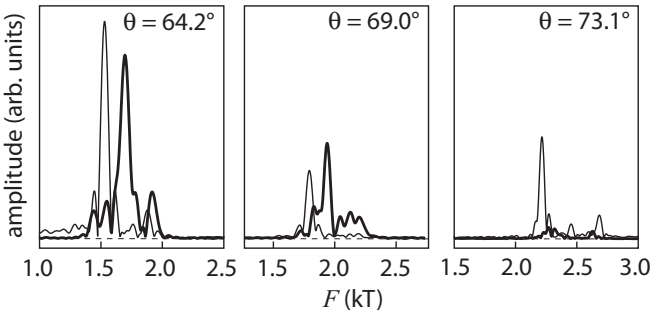

FIG. 10. Fourier transforms of the oscillations below (thin lines) and above (thick lines) the magnetic transition, which at the angles in this figure occurs at $B \sim 10$ T.

incorporated into all plots of sample #1 frequencies presented in this paper.

We take the nonmagnetic Fermi surface to be the parametrized $PdCoO_2$ Fermi surface that was determined in Ref. [10]. The parameters specifying the Fermi surface are the radius of a circular, cylindrical base Fermi surface k_{00}, and then the amplitudes of the corrugations on this base. k_{60}, for example, is the amplitude of the hexagonal distortion. k_{01} sets the difference between the radii of the neck and belly orbits. A thorough description of this system of parametrization is given in Ref. [29].

We allow three parameters to be adjusted, within small ranges that are consistent with experiment, to match the overall levels of the observed $PdCrO_2$ frequencies. We emphasize that this adjustment only tunes the overall levels, and does not substantially alter any of the substructure. These parameters are as follows: (1) the overall size of the Fermi surface (k_{00}), (2) the magnitude of the hexagonal distortion (k_{60}), and (3) the in-plane lattice constant a. The k_z-dependent Fermi surface corrugations (k_{01}, k_{02}, and k_{31}) are left fixed at the amplitudes found for $PdCoO_2$. When k_{60} is adjusted, the higher-order

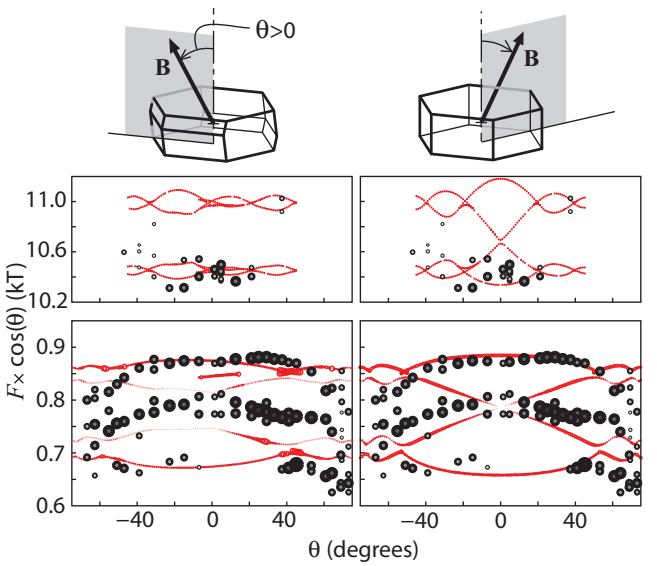

FIG. 11. (Color online) Oscillation frequency against field angle for two further possibilities for the magnetic reconstruction, discussed in the text.

amplitudes $k_{12,0}$ and $k_{18,0}$ are adjusted by hand in response, to smooth the faces and sharpen the corners of the Fermi surface so as to match the Fermi surfaces observed by ARPES [15,16].

The best match is found with $k_{00} = 0.9219$ Å^{-1}, $k_{60} = 0.036$ Å^{-1}, and $a = 2.927$ Å. Further refinement (for example, by allowing a low-temperature lattice distortion, or modification of the k_z-dependent corrugations, or finite avoided crossings) might yield slightly different results: the obtained lattice parameter, for example, is not precisely in line with expectations, as it has been measured to be 2.923 Å at room temperature and some thermal contraction is expected [1]. However, these fitting parameters are within bounds permitted by experiment and are adequate to model the angle dependence.

In addition to the reconstruction shown in the main text, we tested two further possibilities. The first is the same reconstruction but with the other possible orientation relative to the field rotation plane, that the glide plane is rotated from the field rotation plane by 120°. The second tests a hypothetical magnetic zone with vertical side walls, that would preserve the $R\bar{3}m$ symmetry of the nonmagnetic lattice. The results are shown in Fig. 11.

The rotated reconstruction, shown in the left-hand panels in Fig. 11, gives a reasonable match to the data, but not as good as with the glide and rotation planes aligned: it yields the wrong sign on the slope of α_3 against θ, and too low an amplitude on the substructure of the γ_1 frequencies. The $R\bar{3}m$ reconstruction gives a worse match: although it reproduces the α_1 and α_3 frequencies reasonably well, it does not reproduce the structure on γ_1 at all. Therefore, we conclude that the magnetic reconstruction illustrated in Figs. 4 and 5 is the correct one.

[1] H. Takatsu, G. Nénert, H. Kadowaki, H. Yoshizawa, M. Enderle, S. Yonezawa, Y. Maeno, J. Kim, N. Tsuji, M. Takata, Y. Zhao, M. Green, and C. Broholm, Magnetic structure of the conductive triangular-lattice antiferromagnet $PdCrO_2$, Phys. Rev. B **89**, 104408 (2014).

[2] S. Seki, Y. Onose, and Y. Tokura, Spin-driven ferroelectricity in triangular lattice antiferromagnets $ACrO_2$ (A = Cu, Ag, Li, or Na), Phys. Rev. Lett. **101**, 067204 (2008).

[3] Y. Oohara, S. Mitsuda, H. Yoshizawa, N. Yaguchi, H. Kuriyama, T. Asano, and M. Mekata, Magnetic phase transition in $AgCrO_2$, J. Phys. Soc. Jpn. **63**, 847 (1994).

[4] H. Kadowaki, H. Kikuchi, and Y. Ajiro, Neutron powder diffraction study of the two-dimensional triangular lattice antiferromagnet $CuCrO_2$, J. Phys.: Condens. Matter **2**, 4485 (1990).

[5] M. Frontzek, G. Ehlers, A. Podlesnyak, H. Cao, M. Matsuda, O. Zaharko, N. Aliouane, S. Barilo, and S. V. Shiryaev, Magnetic structure of $CuCrO_2$: A single crystal neutron diffraction study, J. Phys.: Condens. Matter **24**, 016004 (2012).

[6] H. Kadowaki, H. Takei, and K. Motoya, Double-Q 120 degrees structure in the Heisenberg antiferromagnet on rhombohedrally stacked triangular lattice $LiCrO_2$, J. Phys.: Condens. Matter **7**, 6869 (1995).

[7] D. Hsieh, D. Qian, R. F. Berger, R. J. Cava, J. W. Lynn, Q. Huang, and M. Z. Hasan, Unconventional spin order in the triangular lattice system $NaCrO_2$: A neutron scattering study, Physica B (Amsterdam) **403**, 1341 (2008).

[8] H. Takatsu, H. Yoshizawa, S. Yonezawa, and Y. Maeno, Critical behavior of the metallic triangular-lattice Heisenberg antiferromagnet $PdCrO_2$, Phys. Rev. B **79**, 104424 (2009).

[9] D. B. Rogers, R. D. Shannon, C. T. Prewitt, and J. L. Gillson, Chemistry of noble metal oxides. III. Electrical transport properties and crystal chemistry of ABO_2, compounds with the delafossite structure, Inorg. Chem. **10**, 723 (1971).

[10] C. W. Hicks, A. S. Gibbs, A. P. Mackenzie, H. Takatsu, Y. Maeno, and E. A. Yelland, Quantum oscillations and high carrier mobility in the delafossite $PdCoO_2$, Phys. Rev. Lett. **109**, 116401 (2012).

[11] V. Eyert, R. Frésard, and A. Maignan, On the metallic conductivity of the delafossites $PdCoO_2$ and $PtCoO_2$, Chem. Mater. **20**, 2370 (2008).

[12] K. P. Ong, Jia Zhang, J. S. Tse, and Ping Wu, Origin of anisotropy and metallic behavior in delafossite $PdCoO_2$, Phys. Rev. B **81**, 115120 (2010).

[13] H. Takatsu, S. Yonezawa, C. Michioka, K. Yoshimura, and Y. Maeno, Anisotropy in the magnetization and resistivity of the metallic triangular-lattice magnet $PdCrO_2$, J. Phys.: Conf. Ser. **200**, 012198 (2010).

[14] Jong Mok Ok, Y. J. Jo, Kyoo Kim, T. Shishidou, E. S. Choi, Han-Jin Noh, T. Oguchi, B. I. Min, and Jun Sung Kim, Quantum oscillations of the metallic triangular-lattice antiferromagnet $PdCrO_2$, Phys. Rev. Lett. **111**, 176405 (2013).

[15] J. A. Sobota, K. Kim, H. Takatsu, M. Hashimoto, S.-K. Mo, Z. Hussain, T. Oguchi, T. Shishidou, Y. Maeno, B. I. Min, and Z.-X. Shen, Electronic structure of the metallic antiferromagnet $PdCrO_2$ measured by angle-resolved photoemission spectroscopy, Phys. Rev. B **88**, 125109 (2013).

[16] Han-Jin Noh, Jinwon Jeong, Bin Chang, Dahee Jeong, Hyun Sook Moon, En-Jin Cho, Jong Mok Ok, Jun Sung Kim, Kyoo Kim, B. I. Min, Han-Koo Lee, Jae-Young Kim, Byeong-Gyu Park, Hyeong-Do Kim, and Seongsu Lee, Direct observation of localized spin antiferromagnetic transition in $PdCrO_2$ by angle-resolved photoemission spectroscopy, Sci. Rep. **4**, 3680 (2014).

[17] H. Takatsu, S. Yonezawa, S. Fujimoto, and Y. Maeno, Unconventional anomalous Hall effect in the metallic triangular-lattice magnet $PdCrO_2$, Phys. Rev. Lett. **105**, 137201 (2010).

[18] H. Takatsu and Y. Maeno, Single crystal growth of the metallic triangular-lattice antiferromagnet $PdCrO_2$, J. Cryst. Growth **312**, 3461 (2010).

[19] The cantilevers are model PRC120, from Seiko Precision Instruments. The sense element is piezoresistive, and the data sheet lists the response, at room temperature, as 16.5 Ω/μm. The spring constant is ≈40 N/m, and the length 120 μm; these parameters can be combined to yield a response to torque of $\approx 3 \times 10^9 \Omega$/N m.

[20] R. D. Shannon, D. B. Rogers, and C. T. Prewitt, Chemistry of noble metal oxides. I. syntheses and properties of ABO_2 delafossite compounds, Inorg. Chem. **10**, 713 (1971).

[21] K. Kimura, H. Nakamura, S. Kimura, M. Hagiwara, and T. Kimura, Tuning ferroelectric polarization reversal by electric and magnetic fields in $CuCrO_2$, Phys. Rev. Lett. **103**, 107201 (2009).

[22] M. Soda, K. Kimura, T. Kimura, and K. Hirota, Domain rearrangement and spin-spiral-plane flop as sources of magnetoelectric effects in delafossite $CuCrO_2$, Phys. Rev. B **81**, 100406(R) (2010).

[23] M. Poienar, F. Damay, C. Martin, J. Robert, and S. Petit, Spin dynamics in the geometrically frustrated multiferroic $CuCrO_2$, Phys. Rev. B **81**, 104411 (2010).

[24] H. Takatsu, S. Yonezawa, S. Mouri, S. Nakatsuji, K. Tanaka, and Y. Maeno, Roles of high-frequency optical phonons in the physical properties of the conductive delafossite $PdCoO_2$, J. Phys. Soc. Jpn. **76**, 104701 (2007).

[25] P. Kushwaha, P. J. W. Moll, N. Nandi, and A. P. Mackenzie, Crystal growth, resistivity and Hall effect of the delafossite metal $PtCoO_2$, arXiv:1411.6162.

[26] K. Kimura, T. Otani, H. Nakamura, Y. Wakabayashi, and T. Kimura, Lattice distortion coupled with magnetic ordering in a triangular lattice antiferromagnet $CuCrO_2$, J. Phys. Soc. Jpn. **78**, 113710 (2009).

[27] A. M. L. Lopes, G. N. P. Oliveira, T. M. Mendonça, J. A. Moreira, A. Almeida, J. P. Araújo, V. S. Amaral, and J. G. Correia, Local distortions in multiferroic $AgCrO_2$ triangular spin lattice, Phys. Rev. B **84**, 014434 (2011).

[28] O. Aktas, G. Quirion, T. Otani, and T. Kimura, First-order ferroelastic transition in a magnetoelectric multiferroic: $CuCrO_2$, Phys. Rev. B **88**, 224104 (2013).

[29] C. Bergemann, A. P. Mackenzie, S. R. Julian, D. Forsythe, and E. Ohmichi, Quasi-two-dimensional Fermi liquid properties of the unconventional superconductor Sr_2RuO_4, Adv. Phys. **52**, 639 (2003).